

Fig. 4. Calculated momentum distributions fit to Ar photoelectron spectra at  $2.6 \times 10^{14}$  W/cm<sup>2</sup>. Curve labels: (a) Model including the lateral distribution, volume and time integration; (b) with lateral distribution, without volume or time integration; (c) with volume and time integration, without lateral distribution; (d) without volume or time integration or lateral distribution.

means taking  $\lim \sigma \rightarrow 0$  in Eq. (5). Curve (c) is therefore the model of Ref. [1] when the field free  $I_p$  and  $Z = 1$  are used. Lastly, curve (d) is the result of a model using only the classical expression for the particle's momentum  $h(I, p) = \delta(p - \sqrt{I}/\omega)$  without any lateral distribution or spatio-temporal integration. In this case, Eq. (7) has an analytical solution,

$$\frac{dN}{dp_y} = \begin{cases} A \frac{\sqrt{I_{avg}/\omega}}{(I_{avg}/\omega^2 - p_y^2)^{1/2}} & |p_y| < \sqrt{I_{avg}/\omega} \\ 0 & \text{else} \end{cases} \quad (8)$$

where  $A$  and  $I_{avg}$  are the fitting parameters.

We note that the two curves including the lateral distribution are very similar. Both closely resemble the measured spectrum. The curves that do not include the lateral distribution are considerably more sharp – even if spatio-temporal integration is included. In the following we show that the lateral distribution is critical for achieving an accurate fit to measurements. We will show that the full model (a) is the best fit, however, model (b) which ignores spatio-temporal integration and uses a single value for the laser intensity is almost as good.

For the H<sub>2</sub><sup>+</sup> experiment, three parameters were used for fitting  $dN/dp_y$ : intensity  $I$ , a constant offset  $B$  to compensate for background signal, and peak height  $A$  to account for gas density, detector efficiency and experimental yield.

$$F(p_y) = A \frac{dN}{dp_y}(I) + B. \quad (9)$$

The experiment collecting photoelectrons used only the two fit parameters  $I$  and  $A$ ; the background was taken as  $B \equiv 0$ . The fitting procedure uses the simplex nonlinear optimization algorithm to minimize the value of the reduced  $\chi^2$  function by varying the fitting parameters. All other values in the algorithm are measured or known (e.g. wavelength, pulse length,  $I_p$ ,  $Z$ ). The goodness of fit is evaluated by the magnitude of the reduced  $\chi^2$  [20].

In Fig. 5 we show how the relation between pulse energy and intensity scales. Below saturation the intensity increases linearly with pulse energy. Once saturation is reached the momentum

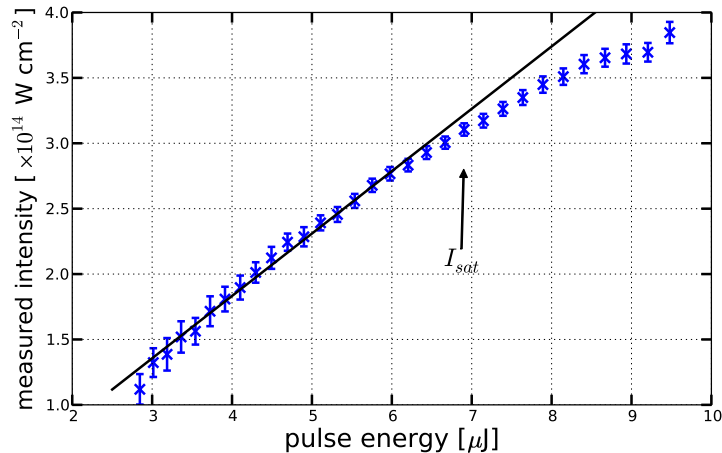


Fig. 5. Relation between pulse energy and measured peak intensity for the electron experiment (15 fs pulse). At low pulse energy the intensity increases linearly with energy. Once saturation is reached, the relationship deviates from linear.

distribution continues to broaden but deviates from the original line.

By fitting to momentum spectra recorded at several different laser intensities we can quantify the accuracy of the fit and identify the relative importance of spatio-temporal averaging and the lateral distribution. At each intensity a photoelectron spectrum was recorded and the four different models were fit to the measurement. The resulting reduced  $\chi^2$  values are shown in Fig. 6. In Fig. 6 there are data markers for each of the four models. The reduced  $\chi^2$  for model (a), including the volume and time integration and lateral momentum distribution, is shown as the blue circles. Model (b), including the lateral distribution but not including spatio-temporal integration, is shown as the green  $\times$  markers and is slightly larger than model (a). However, the reduced  $\chi^2$  values are still quite small for model (b). Also shown are models (c) and (d) as the red triangles and green squares. Models (c) and (d) do not include the lateral distribution and have considerably larger  $\chi^2$  values.

Fig. 6 shows that the best fit – that is, the smallest  $\chi^2$  – is obtained for the full model (a). However, model (b) is very close. Models (c) and (d) which do not include the lateral distribution have substantially larger reduced  $\chi^2$ . This is consistent with Fig. 4 where it is clear that curves (a) and (b) much more closely resemble the measured spectrum.

The agreement of models (a) and (b) illustrates the importance of including the lateral distribution (i.e. the quantum uncertainty) in fitting to the longitudinal momentum distribution. The complete model including the lateral distribution and spatio-temporal integration is the most accurate fit. By comparing the increase in  $\chi^2$  for model (b) to the increase for model (c), we observe that the lateral distribution is of more significance than spatio-temporal averaging. The result for model (b) shows that the distributions can be accurately described by a single laser intensity – ignoring spatio-temporal averaging – provided the quantum mechanical lateral distribution is included.

The goodness of fit is further explained in the inset to Fig. 6. This shows an example of the reduced  $\chi^2$  function for a single spectrum recorded at  $2.55 \times 10^{14} \text{ W cm}^{-2}$ . The inset shows the value of the optimization parameter  $\chi^2$  as a function of the intensity  $I$  used to fit the distribution via Eq. (9). In the inset the intensity is a fitting parameter. It is assumed the minimum  $\chi^2$  corresponds to the true intensity value. We see that the minimum  $\chi^2$  value occurs for model (a) as expected. Model (b) is a slightly less good fit. Models (c) and (d) are poor fits

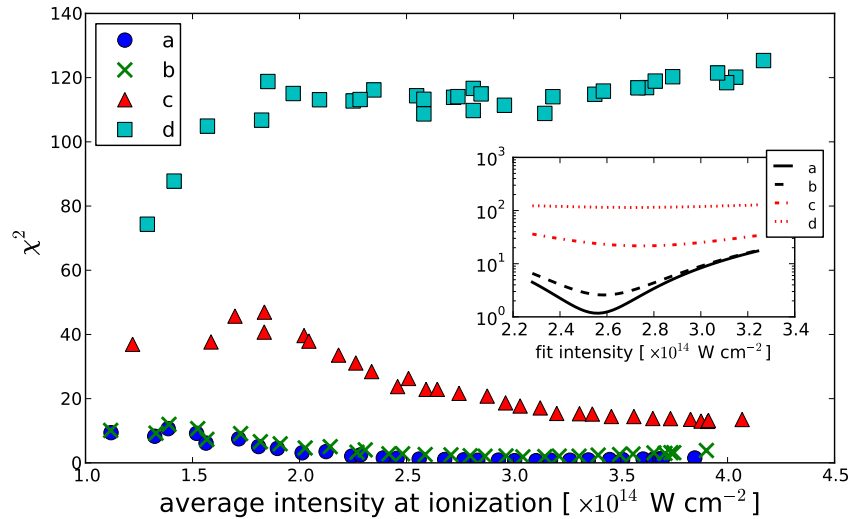


Fig. 6. Goodness of fit for Ar at 800 nm over a range of laser intensities. The reduced  $\chi^2$  statistic is shown for fitting with different models. Inset: Example  $\chi^2$  function for a single spectrum at  $2.55 \times 10^{14} \text{ W cm}^{-2}$ . Model labels: (a) With lateral distribution, volume and time integration; (b) with lateral distribution, without volume or time integration; (c) with volume and time integration, without lateral distribution; (d) without volume or time integration or lateral distribution.

and have  $\chi^2$  values larger by an order of magnitude or more. The substantially larger value of  $\chi^2$  for the models that do not include the lateral distribution illustrates that the lateral distribution is more significant than spatio-temporal averaging. Comparing curves (a) and (b), we see that curve (a) has a very well defined minimum compared to model (b). This is consistent with the results in the main figure. For spectra containing more than  $10^5$  photoelectrons, we estimate the precision of the fit using model (a) is 4% in intensity. Similar results are obtained for fits to other measured spectra. The complete model (a) is the most precise intensity measurement.

In addition to the uncertainty in the the fit, there are other experimental uncertainties associated with momentum calibration (2% in  $\sigma$  and 4% in  $I$ ), laser ellipticity (4% in  $I$ ), detector sensitivity (1% in  $\sigma$ ), and chamber alignment (1% in  $\sigma$ ). When combined with the fit uncertainty, the total accuracy of the intensity measurement is 8%.

In conclusion, strong field ionization with circularly polarized light provides an accurate and sensitive method for measuring the intensity of ultrashort pulses. The pulse must be short enough that the charged particle does not move significantly in the focus. The method can be applied to any gas medium that ionizes in intense fields and works with both positive and negative charged particle detectors. It is robust, and independent of complex molecular fragmentation dynamics that occur in the presence of the strong laser fields. The intrinsic uncertainty of the best model presented here is approximately 4%. We estimate the total uncertainty of the measurement, including systematic errors to be approximately 8%.

### Acknowledgements

CTH acknowledges a NSERC postdoctoral fellowship. CS acknowledges a NSERC postgraduate fellowship. We are pleased to acknowledge funding from NSERC, the Canadian Institute for Photonics Innovations and MURI grant W911NF-07-1-0475.